View metadata, citation and similar papers at core.ac.uk
brought to you by CORE
provided by Bern Open Repository and Information System (BORIS)

Coccolithophore productivity and surface water dynamics in the Alboran Sea during the last 25 kyr

B. Ausín[a]; J-A. Flores[a]; F-J. Sierro[a]; M-A. Bárcena[a]; I. Hernández-Almeida[b]; G. Francés[c]; E. Gutiérrez-Arnillas[c]; B. Martrat[d]; J. O. Grimalt[d] and I. Cacho[e]

[a]Department of Geology, University of Salamanca, La Merced, 37008 Salamanca, Spain.

[b]Institute of Geography and Oeschger Centre for Climate Change Research, University of Bern, Erlachstrasse 9a, CH-3012 Bern, Switzerland.

[c]Department of Marine Geosciences, University of Vigo, Campus As Lagoas – Marcosende, 36310 Vigo, Spain.

[d]Department of Environmental Chemistry. Institute of Environmental Assessment and Water Research, Jordi Girona 18, 08034 Barcelona, Spain.

[e]Department of Stratigraphy, Paleontology and Marine Geosciences, University of Barcelona, Martí i Franquès, 08028 Barcelona, Spain.

Correspondence to: b_ausin@usal.es

Keywords: Coccolithophore productivity, SST, oxygen isotopes, Alboran Sea, Last Glacial Maximum, deglaciation.

source: https://doi.org/10.7892/boris.60892 | downloaded: 27.12.2020

Abstract

Coccolithophore productivity and surface water dynamics for the last 25 kyr in the Alboran Sea (Western Mediterranean) are described in a study of high-resolution sedimentary records from two cores, HER-GC-T1 and CEUTA10PC08, whose locations are currently characterized by different hydrographic conditions. Fossil coccolithophore assemblages and oxygen isotopes and alkenone- and planktonic foraminifera-derived sea surface temperature (SST) records allowed a reconstruction of the properties of the inflowing Atlantic Water (AW), which have proved to be a primary control of the variations in productivity in the neighbourhood of the Strait of Gibraltar. Other local factors, such as fluvial discharge, wind-induced and eddy-induced upwelling, are proposed to have influenced marine productivity in more distant areas. The entrance of cold and less saline AW during the stadials associated with Heinrich Events 2 and 1 prevented primary productivity, which increased along the Last Glacial Maximum, probably due to a greater fluvial discharge. During Terminations 1a and 1b, the upper water column was affected by stratification, although wind-induced upwelling occurred locally. The Bølling-Allerød was characterized by a gradual increase in productivity and the development of the Organic-Rich Layer. Two phases of the Younger Dryas are recognized: a first phase, which was colder, followed by a second phase, which was warmer and wetter. Differences in productivity between both locations during these two phases can be attributed to fluvial discharge and the changing properties of the AW. Local hydrography, such as the dynamics of the western anticyclonic gyre, gained greater importance in determining productivity and its variations during the Holocene, which was the most productive period.

1. Introduction

The Alboran Sea is a transitional region where the Atlantic Water (AW) encounters the Mediterranean Sea. Within its small area, it exhibits most of the physical-biological interaction seen in the open ocean (García-Gorriz and Carr, 1999). Thus, current phytoplankton abundance and distribution in the Alboran Sea are governed directly by: (i) the physical, chemical and

biological properties (rate of flow, SST, salinity content, nutrient concentration, etc.) of the AW that enters the Strait of Gibraltar (Navarro et al., 2011), (ii) the hydrodynamic configurations determined by the Atlantic Jet (AJ) and its two associated gyres, where vertical mixing is a primary factor (Gómez et al., 2000; Echevarría et al., 2002; Navarro et al., 2011) and (iii) upwelling processes determined by the westerly winds blowing along the south Iberian continental shelf (Sarhan et al., 2000; Navarro et al., 2011).

In this study, the variations in primary productivity during the last 25 kyr are described by using fossil coccolithophore assemblages and placing emphasis on local changes.

Because coccolithophores are strongly influenced by nutrient availability, SST and other environmental factors, fossil coccoliths are successfully used as a widespread proxy in paleoproductivity and paleoenvironmental reconstructions (Thierstein and Young, 2004). Apart from the specific biogeography of each species, coccolithophores are sensitive to coastal currents, gyres, eddies, river discharge, and upwelling (Baumann et al., 2005; Guerreiro et al., 2013) and hence their variability in the sedimentary records allows changes in the factors that determine their local production to be tracked over time.

We have studied material from two sites: core CEUTA10PC08, located at the entrance of the Alboran Sea under the direct influence of the incoming AW, and core HER-GC-T1, located off the coast of Malaga under the influence of the semi-permanent productive cell determined by the geostrophic front of the Western Anticyclonic Gyre (WAG) (Ruiz et al., 2001) (Figure 1).

Along with the high-resolution fossil coccolithophore records from these two sites, SST reconstructions (derived from $U^{k'}_{37}$- and MAT- paleothermometers), oxygen isotopes, total concentration of C_{37} alkenones and the *n*-hexacosan-1-ol index were used as tracers of the environment in which coccolithophores proliferated.

Our aim was to identify the local processes determining paleoproductivity in the western Alboran basin for the last 25 kyr, together with the properties of surface (e.g. nutrient availability, temperature and salinity variability) and deep waters (ventilation) in order to gain a comprehensive understanding of the water column dynamics as a whole.

2. Study area and oceanographic setting

The Alboran Sea is the westernmost basin of the Mediterranean Sea, connected to the Atlantic Ocean through the narrow Strait of Gibraltar (Figure 1a). The incoming surface flux of AW (the so-called Atlantic Jet (AJ)) describes two semi-permanent anticyclonic gyres (Figure 1): the Western and the Eastern Anticyclonic Gyres (WAG and EAG, respectively) (Heburn and La Violette, 1990). The AW mixes with surface Mediterranean waters on its way to the east, forming the Modified Atlantic Water (MAW) (0-200 m) (Figure 1b). At depth, Levantine Intermediate Water (LIW) (200-800 m) flows along with Western Mediterranean Deep Water (WMDW) (800-3000 m) in the opposite direction, outflowing as the Mediterranean Outflowing Water (MOW) (Figure 1b). At the northern edges of the anticyclonic gyres, the mixing of AW and MAW produces a frontal system that favors vertical mixing and productive events, forming quasi-permanent areas of upwelling (García-Gorriz and Carr, 1999) (Figure 1a).

3. Materials and Methods

We analyzed two cores in the Alboran Sea: the gravity core HER-GC-T1 (36°22'12''N, 4°17'57''W; taken at 658.9 meters below sea level (mbsl)), and the piston core CEUTA10PC08 (36°1'22''N, 4°52'3''W; 914 mbsl) (Figure 1). Core HER-GC-T1 has a length of 374 cm and consists of dark greenish-gray mud rich in calcareous oozes. Core CEUTA10PC08 is 648 cm long and is mainly composed of brown silt-mudstone.

3.1. Age model

Fifteen radiocarbon ages for core CEUTA10PC08 (Table 1) and seven for core HER-GC-T1 (Table 2) were determined on picked foraminifera shells, using the accelerator mass spectrometry (AMS) technique at the Poznan Radiocarbon Laboratory, the Center for Applied Isotope Studies of University of Georgia, and the Woods Hole Oceanographic Institution. These ^{14}C AMS ages were converted to calibrated calendar years using the OxCal 4.2 online software (Bronk, 2008) and the curve of the calibration dataset Marine13 (Reimer et al., 2013), which includes the correction of 400 yr for the global marine reservoir effect. The regional difference

from this global reservoir correction (ΔR) (Stuiver and Reimer, 1993) resulted in -22 ± 35 years (Siani et al., 2000) and was also considered. All dates reported here are given in calendar ages BP. The age model for core CEUTA10PC08 was based on linear interpolation between these fifteen calendar ages (Table 1), performed with the AnalySeries Version 1.1 (Paillard et al., 1996). This age model covers from 25.5 to 4.5 ka (Figure 2). We assigned an age of 4.5 ka to the core top (0 cm) since we assumed a constant sedimentation rate between the first dated section and the core top. We are aware of the low accuracy of this assumption, but we consider that this is more reliable than assuming an age of 0 ka at a depth of 0 cm. The resulting average sedimentation rate was found to be 37.4 cm kyr^{-1}.

The age model for HER-GC-T1 was also based on a linear interpolation between its respective seven calendar ages (Table 2). Three additional tie points (Table 2) were also considered. These were obtained by correlation between the oxygen isotopic records from this core and core CEUTA10PC08 (Figure 2), since the latter has a more accurate age model. The resulting age model covers from 23.5 to 0.09 ka (Figure 2) and the average sedimentation rate proved to be 16.6 cm kyr^{-1}.

3.2. Coccolithophore assemblage analysis

A total of 297 samples from core CEUTA10PC08 and 143 samples from core HER-GC-T1 were considered for coccolithophore analysis, respectively providing time resolutions of 65 and 165 yr, on average. Samples were prepared following the settling technique of Flores and Sierro (1997). A minimum number of 500 specimens per sample were counted and identified using a Nikon Eclipse 80-i petrographic microscope with a phase contrast device at 1000x magnification. A second count of 20 fields of view was performed in order to accurately estimate the abundance of rare species (those whose relative abundance was less than 1 % in the first count). The Relative abundance (%) and absolute abundance (number of coccoliths g^{-1}) of each species were calculated for all samples. The total absolute abundance (total N) was also calculated in each core as the sum of the absolute abundances of all the taxa in each sample

except reworked specimens. Total N was interpreted as an indicator of coccolithophore productivity.

All species identified and counted in this study have been reported previously in the study area (Weaver and Pujol, 1988; Colmenero-Hidalgo et al., 2004; Álvarez et al., 2010) and are listed in the Appendix. The species *Emiliania huxleyi*, *Gephyrocapsa aperta* and *Gephyrocapsa ericsonii* were lumped together as "small placoliths" (< 3 μm) in this study owing to their common ecological significance (Winter and Siesser, 1994). Reworked specimens were taxa pertaining to older stratigraphic levels (regularly older than the Pliocene in these records), and their abundance was studied via their percentages relative to the other taxa.

According to visual criteria (little or no evidence of dissolution; diagnostic characters fully preserved) (Flores and Marino, 2002) the preservation of the coccoliths is good-to-moderate. The distal shields of some specimens were seen to have been affected by a slight degree of dissolution but this did not complicate their identification.

3.3. Oxygen stable isotopes

Up to 20 well-preserved specimens of the planktonic foraminifer *Globigerina bulloides* were picked from the >150 μm size fraction in 315 samples from core CEUTA10PC08 and in 111 samples from core HER-GC-T1. Individuals were crushed, subjected to ultrasound, and cleaned with methanol before isotopic analyses were performed with a SIRA mass spectrometer at the University of Barcelona. Calibration to the Vienna Pee Dee Belemnite (VPDB) standard scale (Coplen, 1996) was accomplished using the NBS-19 standard, and analytical precision was better than 0.06 ‰ for $\delta^{18}O$.

3.4. Planktonic foraminifera-based SST reconstruction

172 samples from core CEUTA10PC08 were selected and sampled every 4 cm for the analysis of planktonic foraminifera. Samples were first wet-sieved through a 63-μm mesh, and then dry-sieved through a 150-μm mesh. At least 350 specimens from a representative aliquot of the >150 μm sieved fraction were identified in each sample and the relative abundance (%) of the species was calculated.

Multiple SST reconstructions using planktonic foraminifera census counts were performed in order to determine the season and depth at which temperature variability appeared to be the most important for the fossil assemblage from core CEUTA10PC08. On the basis of this foraminifera census we performed a SST reconstruction using the modern analogue technique (MAT) (Prell, 1985). For the calibration we used the 862-site North Atlantic and Mediterranean planktonic foraminifera census counts compiled by Kucera et al. (2005a). Summer, winter and annual ocean temperatures for the calibration set sites were extracted at the 14 standard World Ocean Atlas (Locarnini et al., 2010) depths (between 10 and 500 m), using Ocean Data View software (Schlitzer, 2008). The calculations for MAT were performed using C2 software (Juggins, 2003). The statistical significance of the reconstructions at different depths was tested following the procedure described by Telford et al. (2013) and performed using the palaeoSig package v.1.1-1 (Telford, 2012) for R (R Development Core Team, 2011).

3.5. Molecular biomarkers and $U^{k'}_{37}$-based SST

A set of 114 samples from core HER-GC-T1 was selected for the analysis of fossil organic compounds (long chain alkenones, alcohols and hydrocarbons). A more detailed sampling was carried on the first 2 m of the core, sampled every 2-3 cm, while the remaining 1.5 m of the core was sampled every 5 cm. The experimental procedures used are described in Villanueva et al. (1997). Samples were analyzed with a Varian Gas Chromatograph model 450, a Cold On-Column Injector 1093 and a Flame Ionization Detector. The carrier gas was hydrogen (2.5 mL/min). The identification and quantification of the C_{37} di- and tri-unsaturated alkenones, which are synthesized by coccolithophorid flora, allowed the calculation of the $U^{k'}_{37}$ index. In order to measure SST, this index was calibrated using the equation proposed by Müller et al. (1998). The total concentration of C_{37} alkenones ($[C_{37:2}+C_{37:3}]$) was also calculated. The resistance of vascular plant debris to degradation by oxygenation was examined via the relative ratio between of *n*-hexacosan-1-ol ($C_{26}OH$) and the sum of ($C_{26}OH$) plus *n*-nonacosane (C_{29}) (Martrat et al., 2007). The concentration of each compound was determined using *n*-hexatriacontane as internal standard.

3.6. Statistical analyses

The REDFIT spectral analysis method can be successfully used in unevenly sampled temporal data. PAST 3.01 software (Hammer et al., 2001) uses an implementation of the REDFIT procedure of Schulz and Mudelsee (2002). This method was applied to some of the proxies reported here in order to identify the dominant frequencies of their signals, as well as the red noise and the "false-alarm levels" (95% and 99%) based on parametric Chi-squared approximations at which periodicities are considered significant.

4. Results

4.1. Coccolithophore assemblages

Relative abundances were similar in both cores (Figure 3, 4). Small placoliths comprise up to 90 % of the fossil assemblage in some intervals while their relative abundance decreases to 40 % during the stadials associated with Heinrich Events 2 and 1 (H2 and H1). *Gephyrocapsa muellerae* is relatively more abundant up to H1, while *Gephyrocapsa oceanica* and *Florisphaera profunda* (Figure 3) begin an increasing trend from the Bølling-Allerød (B-A) onwards up-core. The relative abundance of reworked specimens is higher up to the B-A (Figure 3i, j), showing two peaks of up to 25 % during H2 and H1 in core CEUTA10PC08. *Emiliania huxleyi* (> 4 μm), *Helicosphaera* spp., and *Syracosphaera* spp. show coeval peaks of relative abundance during H2 and H1 (Figure 4). The relative abundance of *Oolithotus fragilis* in both cores and of *Umbellosphaera irregularis* in core CEUTA10PC08 peaks during T1a (Figure 4g, h, i). These species undergo an increasing trend from the onset of the YD onwards in both cores.

The absolute abundance of small placoliths increases up-core in both records (Figure 3a, b), except during H2 and H1, where they reach low values. *G. muellerae* shows an increasing trend from 9 ka up-core in core CEUTA10PC08 (Figure 3c), while in core HER-GC-T1, it shows several peaks of high values from 20 to 17.3 ka and from 16.2 to 12.8 ka. *G. oceanica* shows very low values until the onset of Termination 1a (T1a) in both cores (Figure 3e, f). From that time up-core, this species shows an increasing trend in core CEUTA10PC08 while several

peaks of lower values are seen in core HER-GC-T1. The values of *F. profunda* (Figure 3g, h) are very low until the onset of T1b in both cores, showing an increasing trend from 11 ka up-core in core CEUTA10PC08 (Figure 3g) and an increasing trend and large oscillations from 7.7 ka up-core in core HER-GC-T1 (Figure 3h). The absolute abundance of *E. huxleyi* (> 4 μm) peaks at the onset of H2 in core CEUTA10PC08 and shows higher values from 19.5 to 17.5 ka in both cores and during H1 (Figure 4a, b). In core HER-GC-T1 this species also shows a peak during the YD. In core CEUTA10PC08 the absolute abundance of *Helicosphaera* spp. and *Syracosphaera* spp. (Figure 4c, e,) peaks during the H2 and the YD. From the onset of the T1b, *Syracosphaera* spp. displays an increasing trend and high values, while *Helicosphaera* spp. shows several peaks but no remarkable trend. In core HER-GC-T1, the profiles of both species display low values (Figure 4d, f). In core CEUTA10PC08, *O. fragilis* and *Umbellosphaera* spp. (Figure 4g, i) have higher absolute abundances during T1a and show an increasing trend from 12.5 ka up-core, with maximum values between 8.5 and 6.5 ka. In core HER-GC-T1, the absolute abundance of *O. fragilis* shows an increasing trend and high variability from T1a up-core (Figure 4h), while *Umbellosphaera spp.* increases from 10 to 8.4 ka and follows a decreasing trend from that time along the Holocene (Figure 4j).

The total N profiles of both cores (Figure 5d, e) show similar general trends: low values from 25 to 15 ka and a peak at 18.8 ka, an increasing trend and high variability from 15 to 7.5 ka, and high values and marked variability from 7.5 ka up-core. It is worth noting that total N absolute values in core CEUTA10PC08 are double those found in core HER-GC-T1.

4.2. Oxygen Isotope Record

Common overall patterns are observed in both records (Figure 5b): higher values from 23.5 to 17.5 ka, a trend to lower values from 23.5 to 10 ka, and lower values from 10 to 4.5 ka (minimum values being seen at 8 ka). The last 4.5 ka are only available in the oxygen isotopic profile of core HER-GC-T1, which is stabilized and shows no remarkable trend.

With regard to short-term changes, a fast depletion (0.9 ‰) is seen during H2, a period only available in core CEUTA10PC08. In addition, both records are punctuated by depletions at 21

ka (1.6 ‰), at 19 ka (better seen in core CEUTA10PC08), at 16.2 ka during the H1 (0.5 ‰ in core HER-GC-T1 and 0.9 ‰ in core CEUTA10PC08), and at 15 ka during T1a (1.6 ‰).

4.3. Sea Surface Temperature (SST)

4.3.1. Planktonic foraminifera-based SST reconstruction: calibration depth and significance

Planktonic foraminifera live in a broad range of depths in the upper ocean. Therefore, the reconstruction that best explains the variability in the fossil record reflects the depth and season that most influenced the faunal composition. Telford et al. (2013) demonstrated that planktonic foraminifera-based SST reconstructions calibrated against a fixed depth may be biased if the thermal structure of the upper ocean changed over time. We assessed the most suitable calibration depth and season for use in the reconstruction by analysing the proportion of variance in the fossil data explained by reconstructions derived for each of them (Figure 6a).

In order to test the statistical significance of the SST reconstruction in core CEUTA10PC08 we used the method proposed by Telford and Birks (2011). This reconstruction is compared with 999 alternative models trained with random environmental variables. Figure 6a shows that the reconstruction of warm season temperatures at 10 m depth (Figure 6c) explains 39 % of the down-core variance, and indeed explains more variance than the alternative models (95 % significance level at 0.1) (Telford and Birks, 2011). These results may possibly reflect the notion that shallow-dwelling taxa bearing photosynthetic symbionts that are constrained to the upper photic-zone (e.g. *G. bulloides* and *Globigerinoides ruber*) are more abundant in the fossil assemblage, and statistically more significant in the reconstruction. The amount of variance explained by the reconstructions from core CEUTA10PC08 declines with depth (Figure 6a).

Squared chord distances between all modern assemblages were calculated to identify dissimilarities between modern and fossil assemblages. Figure 6b shows that most of the fossil assemblages are below the 5^{th} percentile (minimum dissimilarity) and none are above the 10^{th} percentile (square chord distance of 21.8; non-analogue assemblages) of all distances between calibration set assemblages (Overpeck et al., 1985), indicating good analogue quality for the reconstruction. The highest dissimilarity values are seen around 10 ka and 17 ka.

MAT-estimated summer-SST (Figure 5c) dropped during H2 from 15.2 °C to its minimum value of 10 °C SST, and then increased and oscillated around 15.5 °C during the LGM. Lower values are recorded during H1, while an increase of 6 °C is seen during T1a. SST fell by 2 ºC at the onset of both the B-A and YD and fell again by 4.7 °C at the onset of T1b followed by a rise of 8 ºC from 10.5 to 9.5 ka. During the Holocene, SST oscillated slightly around 22 °C.

4.3.2. Alkenone-based SST reconstruction

The $U^{k'}_{37}$-estimated SST from core HER-GC-T1 (Figure 5c) shows low values from 23.5 ka to the onset of the T1a, its absolute minimum (11.1 °C) being seen at 21.2 ka. During T1a, SST records a fast rise of 3.6 °C and plateaus during the first 1,000 yr of the B-A. SST drops by 2.5 °C at 13.5 ka and shows lower values during the YD followed by a rise of 5.2 °C down to 9 ka, its maximum value being reached (20.1 °C) at that time. From 9 ka up-core, SST records a decreasing, smooth and constant general trend.

4.4. Total concentration of C_{37} alkenones and the n-hexacosan-1-ol index

The total concentration of C_{37} alkenones (Figure 5f) drops from 23.5 to 22.5 ka and during H1. A sharp increase is seen at 15 ka, peaking during the B-A, and showing high values until 9.5 ka. From that time up-core it shows several peaks of low values.

The general trend of the *n*-hexacosan-1-ol index from core HER-GC-T1 (Figure 5g) decreases from 23.5 to 7.5 ka, interrupted by several peaks, such as that observed during the B-A. At 7.5 ka this profile reaches its lowest values, undergoing an increasing trend from that time up-core.

4.5. *Spectral analyses*

Spectral analyses results are shown in Table 3, revealing several centennial and millennial cyclicities significant at the 0.01 and 0.05 confidence levels. Common periodicities (~ 175± 5 yr) for the coccolithophore and the oxygen isotopic records are found in core CEUTA10PC08. This periodicity is not seen in core HER-GC-T1, where SST, oxygen isotopes and some of the coccolithophore records show a different common cyclicity (~ 440± 50 yr).

5. Discussion

5.1. Stadials associated with Heinrich Events 2 and 1 (H2 and H1)

E. huxleyi (> 4 μm) peaks during H2 (only recorded by core CEUTA10PC08) (Figure 4a), as well as during H1 in both cores (Figure 4a, b), pointing to colder conditions, since it is considered a cold SST paleoindicator (Colmenero-Hidalgo et al., 2002; Colmenero-Hidalgo et al., 2004). These peaks are concurrent with a drop of 5.2 °C during H2 (Figure 5c) and decreases of 2 °C and 1.3 °C in core CEUTA10PC08 and core HER-GC-T1, respectively, during H1 (Figure 5c), pointing to a colder SST during these events of northern ice surges.

Peaks of *E. huxleyi* (> 4 μm) match negative excursions of $\delta^{18}O$ from both records (Figure 5b). These isotopic depletions, not expected from the drops in SST, have been extensively explained as low-salinity surface waters entering the Alboran Sea, linked to massive North Atlantic iceberg melting (Cacho et al., 1999; Sierro et al., 2005; Melki, 2011). Smaller peaks of *Syracosphaera* spp. and *Helicosphaera* spp. are seen during these periods (Figure 4c, d, e, f). The absolute abundance of *Syracosphaera* spp. has been reported as a fresh-water input indicator (Bukry, 1974; Weaver and Pujol, 1988), while the isolated appearance of *H. carteri* has been linked to high-productivity waters in other paleoceanographic works (Giraudeau, 1992; Flores et al., 1997), records from sediment traps (Hernández-Almeida et al., 2011) and surface sediment samples (Álvarez et al., 2010). However, this latter statement is at variance with the scant absolute abundance of small placoliths (Figure 3a, b), well-established classic indicators of high-nutrient availability (Okada and Honjo, 1973). We interpreted coeval peaks of *Syracosphaera* spp. and *Helicosphaera* spp. as being linked to the low-salinity inflowing AW. Simultaneous peaks of both species have been interpreted as less saline waters by other authors in the study area (Flores et al., 1997; Colmenero-Hidalgo et al., 2004) and in other latitudes (Álvarez et al., 2005; Flores and Sierro, 2007; Scherer et al., 2008; Maiorano et al., 2009). Thus, it is reasonable to assume that *E. huxleyi* (> 4 μm) would have also found optimal conditions for its development not only in cold but also in low-salinity waters.

The total N from both cores (Figure 5d, e) shows its lowest values, revealing low productivity. This is in agreement with inflowing cold and less saline waters, which are

297 expected to have promoted stratification of the upper layers and hampered upwelling. As a
298 consequence, only *E. huxleyi* (> 4 μm), *Syracosphaera* spp. and *Helicosphaera* spp. would have
299 bloomed.

300 The relative abundance of reworked nannofossils in core HER-GC-T1 shows several peaks
301 but low values between H2 and H1 (Figure 3j), while in core CEUTA10PC08 two striking
302 peaks are seen at the beginning of these stadials (Figure 3i). The different patterns mean that
303 near-bottom redistribution of the material between both locations can be discarded. Downward
304 transport from the exposed continental margin could account for the arrival of reworked
305 material to the HER-GC-T1 core location. This mechanism proved to be useful to explain
306 particle flux distribution in the Malaga area (Fabres et al., 2002; Masqué et al., 2003) and was
307 invoked by Flores et al. (1997) and Colmenero-Hidalgo et al. (2004) to explain the higher
308 relative abundance of reworked specimens during more arid periods in the study area. Although
309 the large peaks of reworked specimens found in core CEUTA10PC08 could be also explained
310 with this mechanism, transport and deposition by deep-water currents is another reasonable
311 interpretation. Located farther from the continental margin, core CEUTA10PC08 was retrieved
312 from an elongated-separated drift that is associated with a moat. Seismic stratigraphic sequences
313 studies show that the acceleration of the deep-water currents eroded the moat, depositing the
314 resuspended material over the core location (pers. com., Ercilla, 2014). In keeping with this
315 hypothesis, Frigola et al. (2008) found high thermohaline circulation during the stadials
316 associated with the Heinrich Events. Nevertheless, it is not possible to rule out downward
317 transport from the continental margin as another likely explanation.

318 The *n*-hexacosan-1-ol index from core HER-GC-T1 (Figure 5g) fell during H1, suggesting
319 higher deep-water ventilation, probably due to high paleocurrent intensity during the early and
320 late phases of the Heinrich Events (Frigola et al., 2008). From 16.2 ka this index underwent an
321 increasing trend, pointing to a worsening of the deep-water ventilation, coeval with an isotopic
322 depletion (Figure 5c), and in line with the slowdown of the thermohaline circulation reported by
323 Sierro et al. (2005) and Frigola et al. (2008) for several Heinrich Events attributed to the entry

of less saline waters. We conclude that these conditions would have affected productivity strongly, encouraging upper water column stratification and preventing the upwelling of nutrient-rich waters during H2 and H1 (Table 4).

5.2. Last Glacial Maximum (LGM)

During this period, defined between 23-19 ka following MARGO (Kucera et al., 2005b), the SST was higher than in the previous H2 and the following H1 (Figure 5c). Productivity rose along the interval at both locations, as shown by higher values of total N (Figure 5d, e). The absolute abundance of *G. muellerae* increased substantially in both records between 21 and 18 ka (Figure 3c, d). Its relative abundance has been used as a cold-water indicator in the study area (Weaver and Pujol, 1988). However, it should be noted that the use of percentages to describe species variability over time must be taken with caution since they are only a relative measure. The lack of agreement among the general patterns of the absolute abundance of G. *muellerae* and SST profiles suggests that the former cannot be controlled only by the latter. Studies from sediment trap samples in the study area (Bárcena et al., 2004; Hernández-Almeida et al., 2011) have revealed the highest fluxes of *G. muellerae* during upwelling periods, controlled directly by colder and highly fertilized waters, as we proposed here. In addition, in core CEUTA10PC08 this rise is coeval with smaller peaks of small placoliths and *H. carteri* (Figure 4c), pointing to productive waters.

From 19.5 to18 ka, peaks of *E. huxleyi* (> 4 μm) are seen in both records (Figure 4a, b), possibly indicating cold and less saline surface waters, as pointed out in section 5.1., via inflowing AW and/or due to the pooling of water from fluvial discharges. Stanford et al. (2011) deduced meltwater release events in northern latitudes at ~19 ka, although their effect in lower latitudes remains unknown. With regard to cold conditions, some authors have found that the Alboran Sea was several degrees colder than the Atlantic side of the Strait of Gibraltar and the eastern Mediterranean basin during the LGM (Hayes et al., 2005; Essallami et al., 2007; Kuhlemann et al., 2008). Owing to the local nature of this cooling, it seems unlikely that inflowing Atlantic waters could account for the bloom of cold and less saline water species,

river discharges being a reasonable explanation. This mechanism is a possible nutrient source in keeping with the enhanced productivity at that time, since less saline waters are expected to favor upper water column stability and hence to hinder the upwelling of deeper waters. We therefore propose that an increase in river discharges would have occurred between 21 and 18 ka, favored by wetter conditions during the LGM (Table 4). This interpretation is in agreement with studies of pollen records (Fletcher and Sánchez Goñi, 2008; Combourieu-Nebout et al., 2009; Fletcher et al., 2010) and model-data comparisons (Kageyama et al., 2005), where the authors report more humid conditions during the LGM in the Alboran Sea as compared with the previous H2 and the following H1.

The C_{37} alkenone profile (Figure 5f) points to an increase in organic matter preservation between 21 and 18 ka, although the *n*-hexacosan-1-ol index (Figure 5g) shows a trend towards increasing deep-water ventilation along this time span. This discrepancy may be due to the aforementioned high productivity that, despite better ventilation of the deep basin, could have hindered the mineralization of organic matter.

5.3. Termination 1a (T1a)

Total N from both cores increases during T1a (Figure 5d, e), indicating increasing productivity, although absolute values are still low. Simultaneous prominent SST rise and oxygen isotope depletion suggest warmer conditions (Figure 5c) coeval with a transition from cold-water coccolithophorid flora (*E. huxleyi* (> 4 μm)) to warm-water and oligotrophic flora: *O. fragilis* and *Umbellosphaera* spp. (McIntyre and Bé, 1967; McIntyre et al., 1970; Okada and Honjo, 1973; Colmenero-Hidalgo et al., 2004) (Figure 4). Interestingly, this transition is more visible in core CEUTA10PC08 (Figure 4a, g, i), where higher the SST matches increases in warm-water taxa. By contrast, in core HER-GC-T1 the peaks of these taxa are smaller (Figure 4h, j) and *G. muellerae* shows a conspicuously increasing trend (Figure 3d), suggesting enhanced productivity.

Two mutually exclusive scenarios are proposed to explain the discrepancies between the CEUTA10PC08 and HER-GC-T1 sites as regard coccolithophore production:

(I) Blowing westerly winds near the coast of Malaga would have induced local upwelling of cold nutrient-rich waters, favoring the blooming of *G. muellerae* and hampering the appearance of warm-water taxa. However, a relatively warm and poor-nutrient AW entering through the Strait would have promoted the increase in oligotrophic and warm-water taxa at the CEUTA10PC08 core location. This configuration is illustrated by the SST satellite images shown in figure 4 in Macías et al. (2008). Regarding this issue, it is worth mentioning that these authors found a significant negative correlation between mean nutrients concentration and the SST.

(II) A northward migration of the AJ along the northern edge of the Alboran Sea would have carried colder and nutrient-rich AW to the HER-GC-T1 core location. By contrast, at the CEUTA10PC08 core location, the warmer and impoverished-nutrient MAW would have allowed the development of warm-water and oligotrophic taxa. The satellite SST images shown in figure 7 in Macías et al. (2008) illustrates this hypothesis.

It is widely accepted that the contemporary hydrographic conditions with distinct geostrophic fronts separating the AJ from ambient Mediterranean waters occurred at around 8 ka (Rohling et al., 1995; Pérez-Folgado et al., 2003; Colmenero-Hidalgo et al., 2004), when the AW inflow rate was close to its present value. Although hypothesis II cannot be discarded, we consider that hypothesis I is a more plausible scenario (Table 4).

The *n*-hexacosan-1-ol index increased until 15 ka (Figure 5g), indicating a weakening of the deep-water ventilation. From 15 ka, the total concentration of C_{37} alkenones shifts to higher values, determining the onset of the well-known organic-rich layer (ORL 1) (Sierro et al., 1998; Cacho et al., 2002; Rogerson et al., 2008) that spans 5,500 yr in our records. Sierro et al., (1998) and Colmenero et al., (2004) described T1a as an interval with a stratified water column due to the input of deglacial waters during the sea-level rise. This scenario would have prevailed across the basin, supporting the notion that the wind-induced upwelling in the HER-GC-T1 area was local.

5.4. Bølling-Allerød (B-A)

405 Total N from both cores shows an increasing general trend, suggesting a rise in productivity
406 along this period (Figure 6d, e). In core CEUTA10PC08, *G. oceanica*, *O. fragilis*, and
407 *Umbellosphaera* spp. (Figure 3e, 4g, i) show higher absolute and relative abundances, while in
408 core HER-GC-T1 the absolute abundance of *G. muellerae* increases substantially (Figure 3d). In
409 the former core, the SST persisted at the same level from 13.5 to 13 ka, while it underwent a
410 decreasing trend in core HER-GC-T1 (Figure 5c). Local factors such as river discharge or local
411 upwelling likely promoted a SST decrease and a productivity rise at the HER-GC-T1 core
412 location off the coast of Malaga, while the CEUTA10PC08 core location conditions remained
413 steady.

414 The total concentration of C_{37} alkenones reached its maximum values along the B-A (Figure
415 5f), indicating the high content and good preservation of organic matter that characterizes the
416 ORL1 (Cacho et al., 2002). This interval corresponds to high insolation (Figure 5a), relatively
417 high SST (Figure 5c), and an impoverishment of the oxygen content in deep seawater as shown
418 by the peak of *n*-hexacosan-1-ol index (Figure 5g) (Table 4). Several authors have reported a
419 similar scenario along with progressively humid conditions, higher river discharge, and a stable
420 water column (Bárcena et al., 2001; Frigola et al., 2008; Fletcher et al., 2010; Rodrigo-Gámiz et
421 al., 2011). These combined conditions, together with increasing productivity along the period,
422 are sufficient to provide organic matter to the sediment and hamper mineralization. However,
423 the process of ORL formation might not necessarily be so simple. Rogerson et al., (2008)
424 studied multiproxy records from four cores in the Alboran Sea and concluded that ORL1
425 formation was due to a combination of reduced-density surface waters and a shoaling of the
426 interface between intermediate and deep waters, while primary productivity was suggested to
427 act as a secondary control.

428 ***5.5. Younger Dryas (YD)***

429 The cooling associated with this interval is marked by a SST drop of 2 °C in core
430 CEUTA10PC08 and lower SST values in core HER-GC-T1 (Figure 5c). In general terms, the
431 total N profiles from both cores show high values pointing to high productivity (Figure 5d, e), in

agreement with previous fossil diatom and coccolithophore records (Bárcena et al., 2001; Colmenero-Hidalgo et al., 2004).

In greater detail, the SST profiles point to the occurrence of two steps during the YD: a first colder one (named here as YDa), from 13 to 12.5 ka, and a second warmer one (YDb), from 12.5 to 11.7 ka. Cool/arid and warm/humid conditions have been respectively invoked to describe the YD as a two-phase interval in the Mediterranean Sea (Cacho et al., 2002; Sbaffi et al., 2004; Combourieu-Nebout et al., 2009; Rodrigo-Gámiz et al., 2011). Coccolithophore abundances and variability also point to both phases, although differing from one core to the other, probably representing more local features than the general superimposed arid/dry and warm/humid conditions.

During YDa, core CEUTA10PC08 reflects a drop in SST (Figure 5c) and in the total N profile (Figure 5d) and coeval peaks of the absolute abundance of *Syracosphaera* spp. and *Helicosphaera* spp. (Figure 4c, e). Such a scenario likely represents the entrance of colder and less saline AW, promoting a steady water column and hampering upwelling pulses. In core HER-GC-T1 total N values drop and then recover at the end of this phase (Figure 5e), while *G. muellerae* shows high absolute abundance (Figure 3d), pointing to a local productivity pulse in that area (Table 4).

During YDb, core CEUTA10PC08 shows higher SST values (Figure 5c), small peaks of warm-water/oligotrophic taxa (Figure 4g, i), and a small drop in the total N profile, although the absolute values are still high (Figure 5d). This was probably due to the entrance of warmer and relatively nutrient-poor AW. Core HER-GC-T1 shows an initial drop in the total N profile, followed by rising values during YDb (Figure 5e). Peaks of *E. huxleyi* (> 4 μm) (Figure 4b) suggest local colder and less saline surface waters, expected to produce upper water column stratification. Therefore, an external nutrient source is necessary to explain the increase in local productivity. A feasible hypothesis would be the discharge of colder waters by rivers flowing into the study area (Guadalfeo River and Guadalhorce River (Figure 1)). Rodrigo-Gámiz et al., (2011) described YDb as a wetter phase affected by an increase in local river discharge with

increased fluvial erosion. In this situation, rivers would account for the nutrient input into the stratified upper water layer, as proposed by Bárcena et al. (2001) from the study of fossil diatom assemblages.

Although the *n*-hexacosan-1-ol index plateaus (Figure 5g) indicate constant deep-water ventilation, C_{37} alkenones decrease gradually (Figure 5f), pointing to thermohaline reactivation, as suggested by previous authors (Sierro et al., 1998; Rodrigo-Gámiz et al., 2011) (Table 4).

5.6. Termination 1b (T1b)

The SST reconstruction from both cores reveals opposite trends and points to a gradient of 5 °C between locations (Figure 5c). However, similar discrepancies have been found on comparing the SST profiles obtained with both methods (alkenones and MAT) from the same core (MD45-2043 in the Alboran Sea) for this period (Pérez-Folgado et al., 2003). Moreover, comparison of $\delta^{18}O$ profiles (Figure 5b) does not reflect substantial offsets. These findings rule out geographical involvement and point to the different nature of the methods (i.e. ecological repercussions from the different planktonic groups employed) used to account for these discrepancies. The isotopic profiles from both cores (Figure 5b) are in agreement with $U^{k'}_{37}$-estimated SST (Figure 5c), while the highest dissimilarity (although still good) between modern and fossil assemblages is seen for the MAT-estimated SST during this period (Figure 6b). It seems likely that the SST drop recorded by the MAT-estimated SST profile would be an understimation inherent to the methodology used.

Nevertheless, total N profiles from both cores (Figure 5d, e) reveal high productivity. The post-glacial sea level rise (Bard et al., 1996) is expected to have prompted a deepening of the nutricline (Colmenero-Hidalgo et al., 2004). Therefore, nutrient input from deeper water layers (i.e. upwelling or vertical mixing) can be discounted as a process responsible for maintaining primary productivity. Eutrophic conditions could have been promoted by a higher rate of inflow of AW enriched in nutrients. The opportunistic and eurithermal small placoliths (Okada and Wells, 1997) would bloom to the detriment of warm-water/oligotrophic taxa, despite the warmer SST (Figure 5c). River runoff is another possible nutrient source, but does not exclude

the previous one. Increased rainfall and more humid conditions during T1b were deduced from geochemical ratios by Frigola et al. (2008). We propose that fertilization by the inflowing AW and/or river discharge would have provided enough nutrients to maintain productivity in the photic zone despite of the stratification of the water column (Table 4).

In agreement with this scenario, the *n*-hexacosan-1-ol index (Figure 5g) increases slightly and the total concentration of C_{37} alkenones levels off (Figure 5f), i.e., deep-water ventilation declines while organic matter preservation remains steady, in keeping with the reduction of the Mediterranean overturning during the T1b (Frigola et al., 2008).

5.7. Holocene

The short-term variability in core HER-GC-T1 for the proxies shown here is discussed in detail in Ausín et al. (submitted for publication). In core CEUTA10PC08, the SST shows an abrupt increase until 9.5 ka and a plateau of high values from that time onwards up-core (Figure 5c). In contrast, a general cooling trend has been reported for the HER-GC-T1 core for the Holocene (Ausín et al., submitted for publication). The SST from CEUTA10PC08, which corresponds to the summer MAT-estimated SST, does not support this cooling trend. These differences may have been due to a more profound effect of seasonality during the Holocene, meaning warmer summers and cooler winters. The MAT-estimated winter and annual SST plotted in figure 6c for comparison, reveals a long-term cooling trend, supporting the notion of an amplification of seasonality. However, this interpretation disagrees with those based on pollen records, which point to cooler summers and warmer winters during this period (Fletcher and Sánchez Goñi, 2008).

Despite the high resolution, none of the proxies from core CEUTA10PC08 shows any striking variability associated with the cold and arid 8.2 ka Event (Alley et al., 1997), suggesting that its repercussions were imperceptible in the Mediterranean context (Wiersma and Renssen, 2006; Zanchetta et al., 2007).

Coccolithophore productivity in core CEUTA10PC08 shows the highest values during the Holocene (Figure 5d), this being the most productive period of the last 25 kyr. The absolute

abundance profiles of most taxa show the same pattern: maximum values between 7.5-6.5 ka and a decreasing trend from then onwards up-core (Figure 3a, c, e and Figure 4e, g, i). In contrast, *F. profunda* shows a constant increasing trend along the whole interval in core CEUTA10PC08 (Figure 3g). This species inhabits the lower photic zone and blooms when the nutricline is located at a deeper position (Molfino and McIntyre, 1990; McIntyre and Molfino, 1996; Beaufort et al., 1997). Its gradual increasing trend along with decreasing values of other taxa suggests a growing stratification of the upper water column close to the Strait of Gibraltar, likely related to a northward migration of the AJ once in the Alboran Sea.

In terms of absolute values, coccolithophore absolute abundances show higher values in core CEUTA10PC08 than in core HER-GC-T1, not only during the Holocene but also over the last 25 kyr (Figure 5d, e). Nevertheless, current productivity distribution in the Alboran Sea is greater at the HER-GC-T1 core location since it is affected by a high-productive cell off the coast of Malaga (Sarhan et al., 2000). This paradox could be explained if the increasing trend of *F. profunda* and decreasing trend of the other taxa seen from 7 to 4.5 ka had persisted for the last 4.5 kyr up-core, implying a more stratified water column characterized by low productivity at the CEUTA10PC08 core location. However, the lack of the last 4.5 ka in core CEUTA10PC08 prevents further interpretation.

During the Holocene, the patterns shown by coccolithophore absolute abundances differ markedly between both locations (Figure 3, 4). The WAG, depicted by a well-defined AJ that flows eastward, is one of the most notable features of the present hydrographic configuration of the Alboran Sea (Figure 1), established at around 8 ka (e.g. Rohling et al., 1995). These surface dynamics entailed new factors influencing primary productivity, such as eddy-induced upwelling at the northern edge of the WAG (Sarhan et al., 2000; Ruiz et al., 2001) where HER-GC-T1 is located. In turn, productivity at the CEUTA10PC08 core location would have been more influenced by the properties of the transitional AW due to its proximity to the Strait of Gibraltar. This configuration was probably responsible for the different patterns of coccolithophore absolute abundances recorded for both cores (Table 4).

5.8. Periodicities

The SST and oxygen isotopes records from core HER-GC-T1 reveal a common periodicity of around 740±20 yr, similar to that of 730± 40 yr observed in a SST record from the Alboran Sea for the Holocene (Cacho et al., 2001). This cyclicity corresponds to the occurrence of short-term cooling events transmitted to the Mediterranean by Atlantic inflowing waters during the Holocene. Nevertheless, CEUTA10PC08 does not show such periodicity, despite being located closer to the Atlantic. Cacho et al. (2001) have reported an amplifying effect of these cooling events eastwards along the Mediterranean due to intense winds, which could account for the lack of such cyclicity in core CEUTA10PC08.

Spectral analyses do not reveal common periodicities between the two studied cores and, except for that of 740±20 yr mentioned above, to our knowledge no similar cycles have been found in nearby cores in the study area nor in the Atlantic Ocean for the last 25 kyr. Rodrigo-Gámiz et al. (2014) identified significant cycles of 1300, 1515, 2000, and 5000 yr and secondary harmonics of 650, 1087, and 3000 yr in a core from the Western Mediterranean for the last 20 kyr. These periodicities have been associated with solar activity, monsoonal regimes, orbital forcing, oceanic-atmospheric processes related to North Atlantic climate variability and African monsoon systems. Nevertheless, the authors stated that only periodicities between 500 and 7000 yr have been interpreted since cyclicities outside that range could be simply a consequence of the method employed owing to the time span and the sampling interval considered, similar to those considered here. None of the above periodicities match that of ~ 175± 5 yr frequently found in the records of core CEUTA10PC08 or of ~ 440± 50 yr in several records of core HER-GC-T1, suggesting that the processes that took place at both locations would have been affected by several not necessarily common forcing mechanisms, possibly of local nature.

6. Conclusions

According to the results of the present work, coccolithophores are highly sensitive to local hydrographic and environmental conditions. From the study of two oceanic cores, it may be concluded that the Atlantic water entering the Alboran Sea would have exerted primary control over productivity in the areas close to the entrance of the Strait of Gibraltar during the last 25 kyr. Their physical and biological properties (rate of inflow, nutrients, temperature and salinity) are seen to have determined the stability of the upper water column as well as the environment in which coccolithophores bloom. On its way to the east, this effect was partly diluted and hence productivity in more distant locations would also have been affected by nutrient input from river discharges, wind-induced upwelling, and specific hydrographic configurations.

As summarized in Table 4, coccolithophore records in combination with other paleoenvironmental proxies have allowed primary productivity variations and water column dynamics to be determined for the last 25 kyr in the Alboran Sea:

During H2 and H1, entering cold and less saline waters prompted the stratification of the water column and prevented primary productivity.

Increased river discharge is proposed from 21 to 18 ka to explain the cold and less saline waters in the study area as well as the enhanced productivity.

Phases T1a and T1b of the deglaciation were characterized by a stratified upper water column, although this did not hamper local wind-induced upwelling.

The B-A is marked by a slight increase in productivity and the development of the ORL.

The YD had two phases: a colder first phase followed by a second, warmer and wetter phase. The properties of the inflowing AW and river discharges were responsible for the differences in productivity between both locations during these two phases.

Productivity increased markedly during the Holocene. The hydrographic configuration during this period, which persists today, played an important role in its productivity and its variations.

Table 1**.** Age model for core CEUTA-10-PC-08. ^{14}C AMS ages measured at Poznan Radiocarbon Laboratory[a]. ^{14}C AMS ages measured at Center for Applied Isotope Studies of University of Georgia[b].

Laboratory code	**Foram type**	**Depth (cm)**	**Radiocarbon age (a)**	**Calendar age (a cal BP)**
CEUTA10PC08_22/ Poz-56516[a]	*G. inflata*	22	5870 ± 40	6312 ± 56
CEUTA10PC08_46/ Poz-56517[a]	*N. pachyderma* (r.c.)	46	7940 ± 40	8426 ± 56
CEUTA10PC08_82/ Poz-56518[a]	*N. pachyderma* (r.c.)	82	9190 ± 50	10006 ± 100
9977[b]	*N. pachyderma* (r.c.)	122	9900 ± 30	10885 ± 91
9552[b]	*G. bulloides*	156	11410 ± 30	12890 ± 79
10602[b]	*N. pachyderma* (r.c.)	174	12240 ± 70	13717 ± 107
9979[b]	*N. pachyderma* (r.c.)	281.5	14270 ± 40	16818 ± 125
9980[b]	*N. pachyderma* (r.c.)	323.5	14920 ± 40	17720 ± 97
9981[b]	*N. pachyderma* (r.c.)	406	16910 ± 40	19936 ± 104
9982[b]	*N. pachyderma* (r.c.)	452	18110 ± 50	21462 ± 128
9983[b]	*N. pachyderma* (r.c.)	474	18360 ± 50	21773 ± 106
9984[b]	*N. pachyderma* (r.c.)	541.5	20170 ± 50	23820 ± 115
10603[b]	*G. bulloides*	579.5	20480 ± 60	24162 ± 113
10604[b]	*G. bulloides*	603.5	21100 ± 60	24967 ± 173
10605[b]	*N. pachyderma* (r.c.)	615.5	21540 ± 60	25500 ± 111

Table 2. Age model for core HER-GC-T1. ^{14}C AMS ages measured at Poznan Radiocarbon Laboratory[a]. ^{14}C AMS ages measured Woods Hole Oceanographic Institution[b]. Tie points obtained from correlation of oxygen isotopic records[c].

(Sample/Laboratory code)	**Foram Type**	**Depth (cm)**	**Radiocarbon age (a)**	**Calendar age (a cal. BP)**
SEC1_2/ Poz-53233[a]	*G. inflata*	2	440 ± 25	88 ± 62
SEC1_21/OS-87586[b]	*G. inflata*	21	1810 ± 25	1379 ± 54
SEC1_63/ Poz-53234[a]	*G. inflata*	63	4175 ± 35	4284 ± 76
SEC2_17/ Poz-53235[a]	*G. inflata*	107	6100 ± 40	6550 ± 68
SEC2_54/OS-87587[b]	*G. inflata*+*N. pachyderma* (r.c.)	144	7350 ± 35	7834 ± 58
SEC3_12/ Poz-53236[a]	*N. pachyderma* (r.c.)	202	10400 ± 60	11539 ± 162
SEC3_48[c]		238		14582
SEC3_67[c]		257		15217
SEC3_77[c]		267		16198
SEC3_92/Poz-53237[a]	*N. pachyderma* (r.c.)	282	15180 ± 80	18006 ± 121
SEC4_36[c]		326		21396

Table 3. Periodicities (given in years and separated by semicolons) resulting from the spectral analyses showing statistical significance at the 95 and at 99 confidence levels (%) from core CEUTA10PC08 and core HER-GC-T1.

	Core CEUTA10PC08		**Core HER-GC-T1**	
Record	**95%**	**99%**	**95%**	**99%**
small placoliths	10000	308; 185; 174	760	11700
G. oceanica	185; 171	215; 148		341
G. muellerae		5000; 179		5800; 428; 399
F. profunda		10000; 176	3900	11000; 360; 346
Syracosphaera spp.		10000; 183, 171	7800; 427; 341	
Helicosphaera spp.	5000	195	636	427; 412
Oxygen isotopes	7000	180; 173	1000	725; 416
SST		7000; 303; 275		758; 534; 489

Table 4. Summary of the main results and general interpretation. H2 and H1: stadials associated with Heinrich events 2 and 1; LGM: Last Glacial Maximum; T1a: Termination 1a; B-A: Böling-Allerød; YD: Younger Dryas. AW: Atlantic Water. DW: Deep water.

Age (ka cal. BP)	25	23.8	17.5	15.5	23	19	15.5		14.6		13		12.5		11.7		10	0
Interval	H2 and H1				LGM		T1a		B-A		YDa		YDb		← Holocene → T1b			
Specific location							Ceuta	Malaga	Ceuta	Malaga	Ceuta	Malaga	Ceuta	Malaga				
Total N	Drop (lowest values)				Rise but low values		Rise		Drop and rise	Rise	Drop	Drop and rise	Drop, but still high values	Drop and rise	Rise		Rise (highest values)	
Coccolithophore species	Peaks of *E. huxleyi* (> 4 µm), *Syracosphaera* spp. and, *Helicosphaera* spp.				Peaks of *G.muellerae* and *E.huxleyi* (> 4 µm)		Peaks of *O. fragilis* and *U.irregularis*	Peaks of *G. muellerae*	Peaks of *G. oceanica*, *O. fragilis*, and *U.irregularis*	Peaks of *G. muellerae*	Peaks of *Syracosphaera* spp. and *Helicosphaera* spp.	Peaks of *G.muellerae*	Peaks of *O.fragilis* and *U.irregularis*	Peaks of *E. huxleyi* (> 4 µm)	Increase in all taxa		Peaks of all taxa Gradual increase in *F. profunda*	
SST and $\delta^{18}O$	SST Drop $\delta^{18}O$ depletion				SST rise but low values		SST rise		SST rise	SST steady and drop	SST drop		SST rise		SST rise		Long-term cooling trend	
n-hexacosan-1-ol index	Drop				Drop		Rise		Rise		Steady		Steady		Rise			
Total concentration of C_{37} alkenones					Rise		Rise		Rise (highest values)		Drop		Drop		Steady			
Interpretation	Less saline and cold AW Stratified upper water column hampers productivity High DW ventilation				Less saline surface waters: steady upper water column Nutrient input by fluvial dischages: enhanced productivity Good DW ventilation		Warmer AW Bloom of warm-water/oligotrophic taxa	Local wind-induced upwelling Onset of the ORL1	Warmer AW Bloom of warm-water/oligotrophic taxa Development of the ORL1	Colder surface waters Local upwelling (by river discharge or wind-induced upwelling)	Less saline and colder AW hampers productivity	Colder surface waters Local productive pulse	Warmer and poor-nutrient AW Bloom of warm-water/oligotrophic taxa Thermohaline reactivation	Colder and less saline surface water Stratified upper water column Productive pulse due to fluvial input	Warm conditions Productive events Reduction in thermohaline circulation		Gradual stratification of the water column close to the Strait and productive pulses influenced by hydrographic configuration	

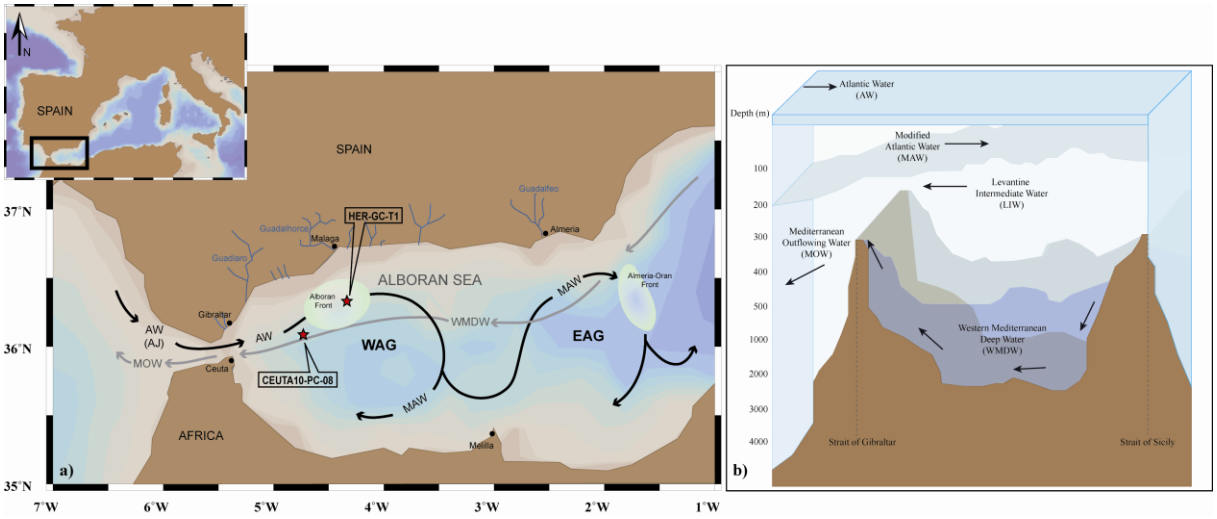

Figure 1. Current oceanographic setting in the Alboran Sea. a) Locations of cores CEUTA10PC08 and HER-GC-T1. Black arrows trace the general surface circulation. Grey arrows trace general deep circulation. b) Vertical distribution of the water masses in the Western Mediterranean. AW: Atlantic Water, entering the Alboran Sea as the Atlantic Jet: AJ. MAW: Modified Atlantic Water. WMDW: Western Mediterranean Deep Water. MOW: Mediterranean Outflowing Water. WAG: Western Anticyclonic Gyre. EAG: Eastern Anticyclonic Gyre.

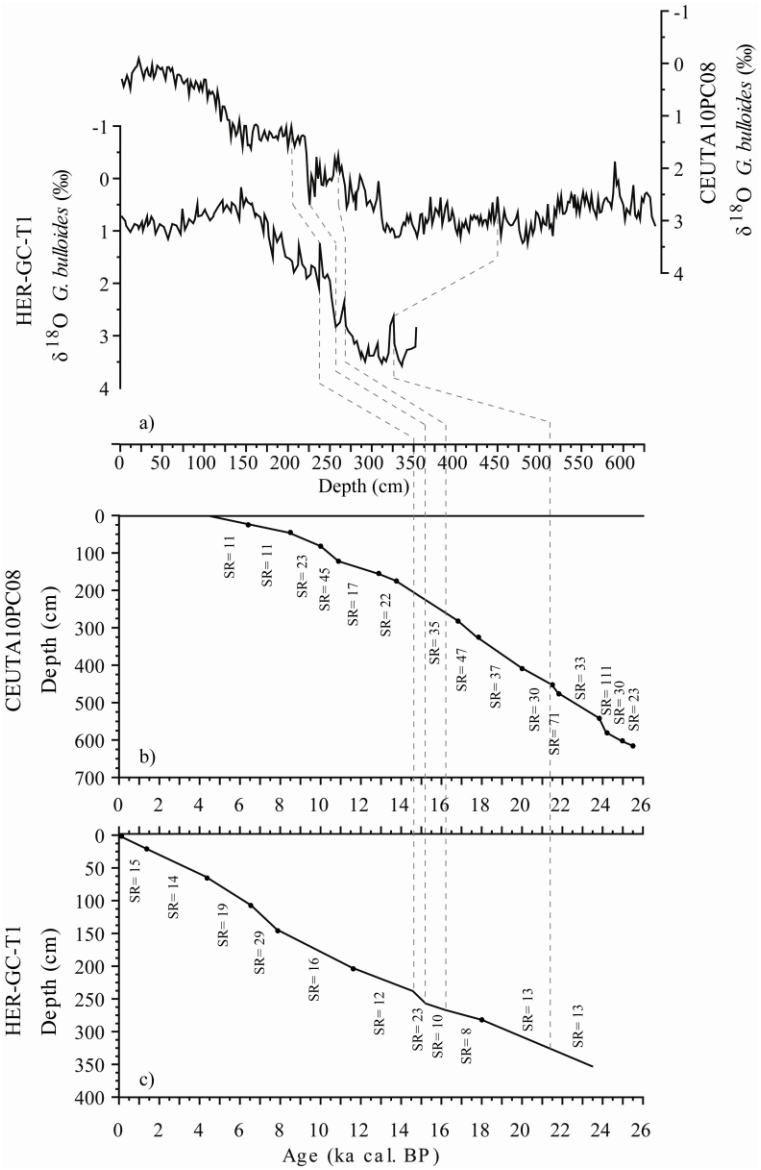

Figure 2. a) Oxygen isotope profiles from cores CEUTA10PC08 and HER-GC-T1. Dashed grey lines join tie points obtained from correlation of both profiles. Age-depth models from core CEUTA10PC08 (b) and core HER-GC-T1 (c). SR stands for sedimentation rate, given in cm kyr^{-1}.

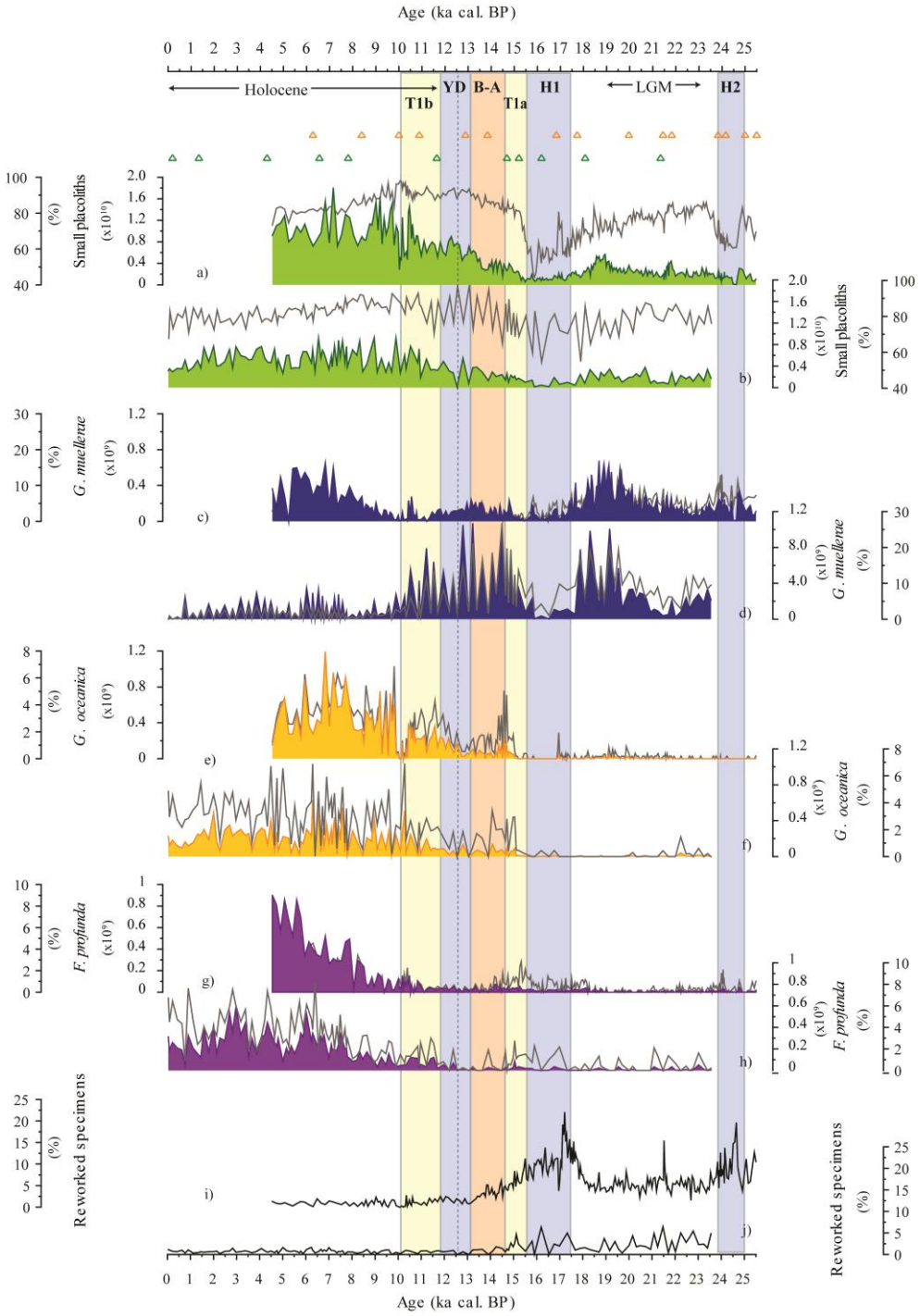

Figure 3. Colored logs represent absolute abundances of the main species (given in number of coccoliths g^{-1}) of the nannofossil assemblages from CEUTA10PC08 (left axes) and HER-GC-T1 (right axes). The relative abundances (given in %) of each species are represented by a dark grey solid line. H2 and H1: stadials associated with Heinrich events 2 and 1; LGM: Last Glacial Maximum; T1a: Termination 1a; B-A: Böling-Allerød; YD: Younger Dryas. The dashed grey

bar separates the YDa and YDb phases; T1b: Termination 1b. Triangles stand for age control points (kyr cal. BP) for core CEUTA10PC08 (orange) and core HER-GC-T1 (green).

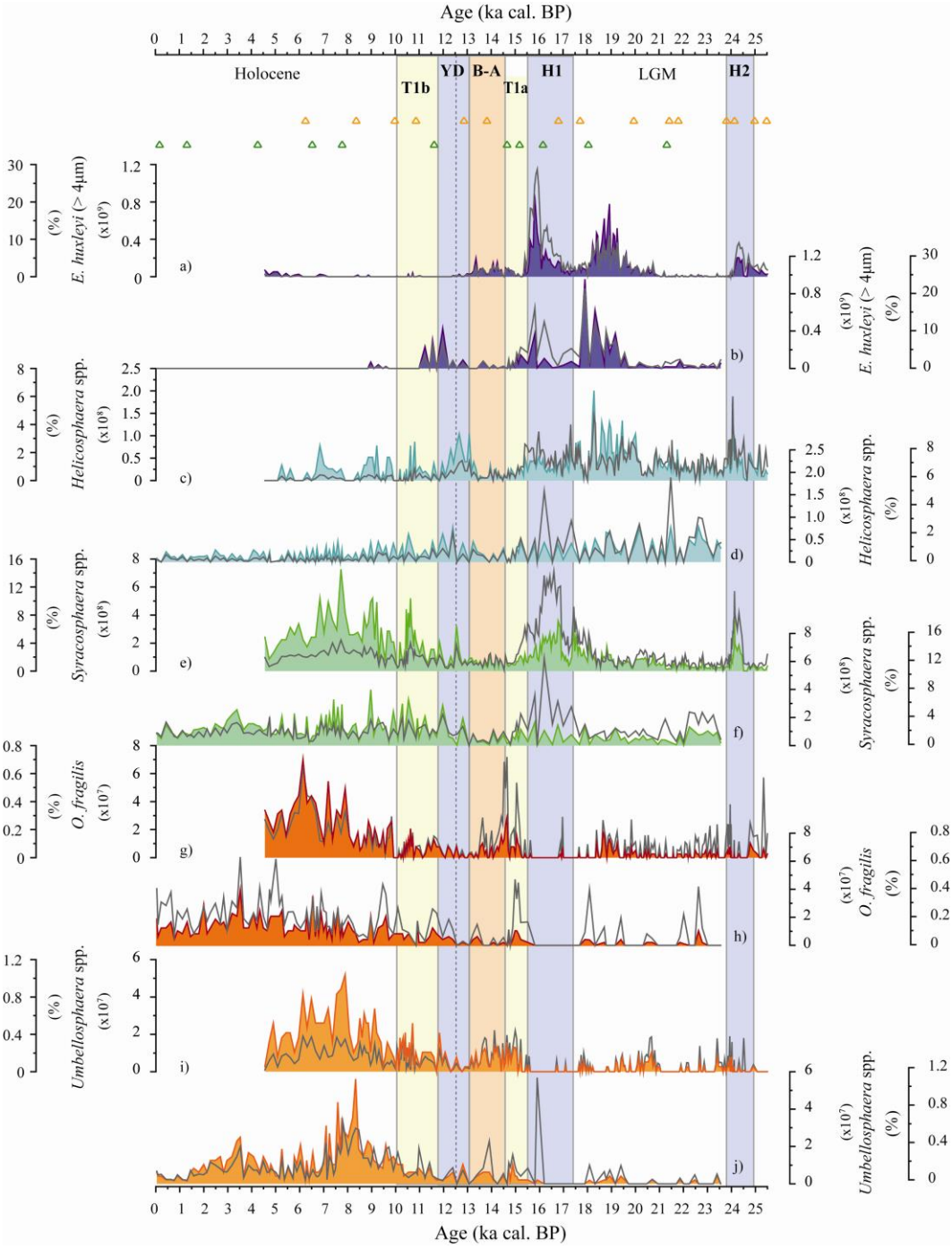

Figure 4. Absolute abundances (colored logs) of the main nannofossil species (given in number of coccoliths g^{-1}) from CEUTA10PC08 (left axes) and HER-GC-T1 (right axes). The relative abundances (given in %) of each species are represented by a dark grey solid line. Triangles stand for age control points for core CEUTA10PC08 (orange) and core HER-GC-T1 (green).

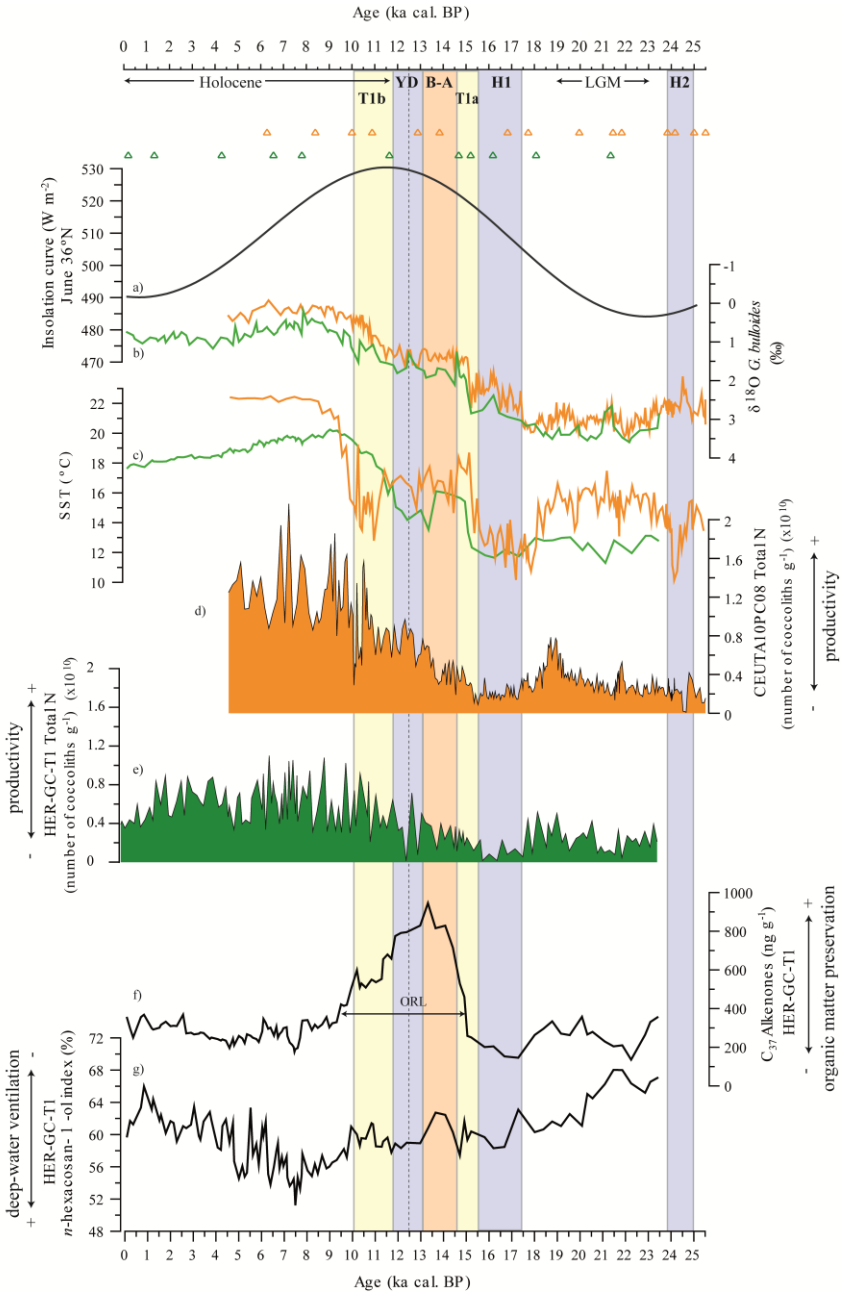

Figure 5. a) Insolation curve (June, 36°N) (Berger, 1978). b) $\delta^{18}O$ record from core CEUTA10PC08 (orange) and core HER-GC-T1 (green) (Note that the vertical axis is reversed). c) MAT-estimated SST (summer season, 10 m depth) of core CEUTA10PC08 (orange) and Uk'37-estimated SST from core HER-GC-T1 (green). d) Total N (total absolute abundance) from core CEUTA10PC08. e) Total N from core HER-GC-T1 f) Concentration of C37 alkenones ([C37:2+C37:3]) from core HER-GC-T1. g) *n*-hexacosan-1-ol index from core HER-GC-T1. ORL: Organic Rich Layer. Triangles stand for age control points for core CEUTA10PC08 (orange) and core HER-GC-T1 (green).

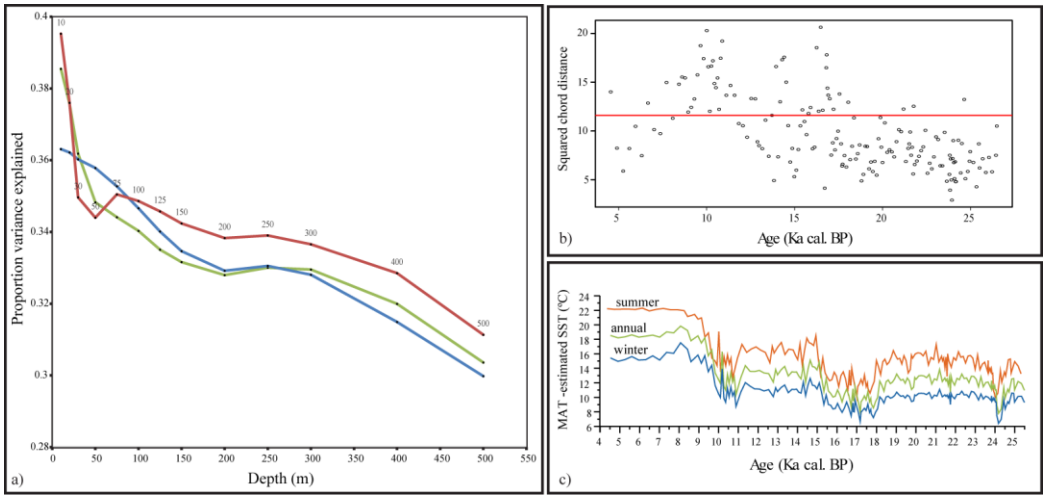

Figure 6. a) Proportion of variance in the fossil data explained by the reconstructions of summer (red), annual (green) and winter (blue) temperatures at different water depths. The 95 % significance level is assessed at 0.1 by finding the proportion of variance explained by reconstructions of random environmental data. b) Dissimilarity between modern and core CEUTA10PC08 fossil assemblages measured by squared chord distance, plotted against age (ka cal. BP). The red line represents the 5th percentile. c) Summer, annual and winter SST reconstructions at 10 m water depth.

Acknowledgements

B. Ausín is sincerely grateful to Y. González and B. Hortelano (Department of Environmental Chemistry, IDAEA-CSIC, Barcelona) for their guidance and supervision during the geochemical analyses. This study was supported by the FPU grant AP2010-2559 of the Ministry of Education of Spain awarded to B. Ausín and by the Consolider Ingenio "GRACCIE" program CSD 2007-00067, the program CGL2011-26493 and VACLIODP339, CTM2008-06399-C04/MAR and CTM2012-39599-03-01 projects of the Spanish Ministry of Science and Innovation.

References

Álvarez, M.C., Amore, F.O., Cros, L., Alonso, B. and Alcántara-Carrió, J., 2010. Coccolithophore biogeography in the Mediterranean Iberian margin. Revista Española de Micropaleontología, 42: 359-372.

Álvarez, M.C., Flores, J.A., Sierro, F.J., Diz, P., Francés, G., Pelejero, C. and Grimalt, J., 2005. Millennial surface water dynamics in the Ría de Vigo during the last 3000 years as revealed by coccoliths and molecular biomarkers. Palaeogeography, Palaeoclimatology, Palaeoecology, 218: 1-13.

Alley, R.B., Mayewski, P.A., Sowers, T., Stuiver, M., Taylor, K.C. and Clark, P.U., 1997. Holocene climatic instability: A prominent, widespread event 8200 yr ago. Geology, 25: 483-486.

Ausín, B., Flores, J.-A., Sierro, F.J., Cacho, I., Hernández-Almeida, I., Martrat, B. and Grimalt, J.O., 2014. Atmospheric patterns driving Holocene productivity in the Alboran Sea (Western Mediterranean): a multiproxy approach. Holocene. (Submitted for publication).

Bárcena, M.A., Cacho, I., Abrantes, F., Sierro, F.J., Grimalt, J.O. and Flores, J.A., 2001. Paleoproductivity variations related to climatic conditions in the Alboran Sea (western Mediterranean) during the last glacial-interglacial transition: the diatom record. Palaeogeography, Palaeoclimatology, Palaeoecology, 167: 337-357.

Bárcena, M.A., Flores, J.A., Sierro, F.J., Pérez-Folgado, M., Fabres, J., Calafat, A. and Canals, M., 2004. Planktonic response to main oceanographic changes in the Alboran Sea (Western Mediterranean) as documented in sediment traps and surface sediments. Marine Micropaleontology, 53: 423-445.

Bard, E., Hamelin, B., Arnold, M., Montaggioni, L., Cabioch, G., Faure, G. and Rougerie, F., 1996. Deglacial sea-level record from Tahiti corals and the timing of global meltwater discharge. Nature, 382: 241-244.

Baumann, K.H., Andruleit, H., Boeckel, B., Geisen, M. and Kinkel, H., 2005. The significance of extant coccolithophores as indicators of ocean water masses, surface water temperature, and palaeoproductivity: a review. Palaeontologische Zeitschrift, 79: 93-112.

Beaufort, L., Lancelot, Y., Camberlin, P., Cayre, O., Vincent, E., Bassinot, F. and Labeyrie, L., 1997. Insolation Cycles as a Major Control of Equatorial Indian Ocean Primary Production. Science, 278: 1451-1454.

Berger, A., 1978. Long-Term Variations of Daily Insolation and Quaternary Climatic Changes. Journal of the Atmospheric Sciences, 35: 2362-2367.

Bronk, R.C., 2008. Deposition models for chronological records. Quaternary Science Reviews, 27: 42-60.

Bukry, D., 1974. Coccoliths as paleosalinity indicators -evidence from the Black Sea. Memoirs of the America Association of Petroleum Geologists, 20: 353-363.

Cacho, I., Grimalt, J.O. and Canals, M., 2002. Response of the Western Mediterranean Sea to rapid climatic variability during the last 50,000 years: a molecular biomarker approach. Journal of Marine Systems, 33-34: 253-272.

Cacho, I., Grimalt, J.O., Canals, M., Sbaffi, L., Shackleton, N.J., Schönfeld, J. and Zahn, R., 2001. Variability of the western Mediterranean Sea surface temperature during the last 25,000 years and its connection with the Northern Hemisphere climatic changes. Paleoceanography, 16: 40-52.

Cacho, I., Grimalt, J.O., Pelejero, C., Canals, M., Sierro, F.J., Flores, J.A. and Shackleton, N., 1999. Dansgaard-Oeschger and Heinrich Event Imprints in Alboran Sea Paleotemperatures. Paleoceanography, 14: 698-705.

Colmenero-Hidalgo, E., Flores, J.-A. and Sierro, F.J., 2002. Biometry of Emiliania huxleyi and its biostratigraphic significance in the Eastern North Atlantic Ocean and Western Mediterranean Sea in the last 20,000 years. Marine Micropaleontology, 46: 247-263.

Colmenero-Hidalgo, E., Flores, J.-A., Sierro, F.J., Bárcena, M.Á., Löwemark, L., Schönfeld, J. and Grimalt, J.O., 2004. Ocean surface water response to short-term climate changes revealed by coccolithophores from the Gulf of Cadiz (NE Atlantic)

and Alboran Sea (W Mediterranean). Palaeogeography, Palaeoclimatology, Palaeoecology, 205: 317-336.

Combourieu-Nebout, N., Peyron, O., Dormoy, I., Desprat, S., Beaudouin, C., Kotthoff, U. and Marret, F., 2009. Rapid climatic variability in the west Mediterranean during the last 25 000 years from high resolution pollen data. Clim. Past, 5: 503-521.

Coplen, T.B., 1996. Editorial: More uncertainty than necessary. Paleoceanography, 11: 369-370.

Echevarría, F., García Lafuente, J., Bruno, M., Gorsky, G., Goutx, M., González, N., García, C.M., Gámez, F., Vargas, J.M., Picheral, M., Striby, L., Varela, M., Alonso, J.J., Reul, A., Cózar, A., Prieto, L., Sarhan, T., Plaza, F. and Jiménez-Gámez, F., 2002. Physical-biological coupling in the Strait of Gibraltar. Deep Sea Research Part II: Topical Studies in Oceanography, 49: 4115-4130.

Essallami, L., Sicre, M.A., Kallel, N., Labeyrie, L. and Siani, G., 2007. Hydrological changes in the Mediterranean Sea over the last 30,000 years. Geochemistry, Geophysics, Geosystems, 8: Q07002.

Fabres, J., Calafat, A., Sanchez-Vidal, A., Canals, M. and Heussner, S., 2002. Composition and spatio-temporal variability of particle fluxes in the Western Alboran Gyre, Mediterranean Sea. Journal of Marine Systems, 33-34: 431-456.

Fletcher, W.J. and Sánchez Goñi, M.F., 2008. Orbital- and sub-orbital-scale climate impacts on vegetation of the western Mediterranean basin over the last 48,000 yr. Quaternary Research, 70: 451-464.

Fletcher, W.J., Sánchez Goñi, M.F., Allen, J.R.M., Cheddadi, R., Combourieu-Nebout, N., Huntley, B., Lawson, I., Londeix, L., Magri, D., Margari, V., Müller, U.C., Naughton, F., Novenko, E., Roucoux, K. and Tzedakis, P.C., 2010. Millennial-scale variability during the last glacial in vegetation records from Europe. Quaternary Science Reviews, 29: 2839-2864.

Flores, J.A. and Marino, M., 2002. Pleistocene calcareous nannofossil stratigraphy for ODP Leg 177 (Atlantic sector of the Southern Ocean) Marine Micropaleontology, 45: 191-224.

Flores, J.A. and Sierro, F.J., 1997. Revised technique for calculation of calcareous nannofossil accumulation rates. Micropaleontology, 43: 321-324.

Flores, J.A. and Sierro, F.J., 2007. Pronounced mid-Pleistocene southward shift of the Polar Front in the Atlantic sector of the Southern Ocean. Deep Sea Research II, 54: 2432–2442.

Flores, J.A., Sierro, F.J., Frances, G., Vazquez, A. and Zamarreno, I., 1997. The last 100,000 years in the western Mediterranean: sea surface water and frontal dynamics as revealed by coccolithophores. Marine Micropaleontology, 29: 351–366.

Frigola, J., Moreno, A., Cacho, I., Canals, M., Sierro, F.J., Flores, J.A. and Grimalt, J.O., 2008. Evidence of abrupt changes in Western Mediterranean Deep Water circulation during the last 50 kyr: A high-resolution marine record from the Balearic Sea. Quaternary International, 181: 88–104.

García-Gorriz, E. and Carr, M.E., 1999. The climatological annual cycle of satellite-derived phytoplankton pigments in the Alboran Sea: a physical interpretation. Geophysical Research Letters, 26: 2985-2988.

Giraudeau, J., 1992. Distribution of Recent nannofossils beneath the Benguela system: Southwest African continental margin. Marine Geology, 108: 219-237.

Gómez, F., Echevarría, F., García, C.M., Prieto, L., Ruiz, J., Reul, A., Jiménez-Gómez, F. and Varela, M., 2000. Microplankton distribution in the Strait of Gibraltar: coupling between organisms and hydrodynamic structures. Journal of Plankton Research, 22: 603-617.

Guerreiro, C., Oliveira, A., de Stigter, H., Cachão, M., Sá, C., Borges, C., Cros, L., Santos, A., Fortuño, J.-M. and Rodrigues, A., 2013. Late winter coccolithophore bloom off central Portugal in response to river discharge and upwelling. Continental Shelf Research, 59: 65-83.

Hammer, Ø., Harper, D.A.T. and Ryan, P.D., 2001. PAST: Paleontological statistics software 656 package for education and data analysis. Palaeontologia Electronica, 4: 9.

Hayes, A., Kucera, M., Kallel, N., Sbaffi, L. and Rohling, E.J., 2005. Glacial Mediterranean sea surface temperatures based on planktonic foraminiferal assemblages. Quaternary Science Reviews, 24: 999-1016.

Heburn, G.W. and La Violette, P.E., 1990. Variations in the Structure of the Anticyclonic Gyres Found in the Alboran Sea. Journal of Geophysical Research, 95: 1599-1613.

Hernández-Almeida, I., Bárcena, M.A., Flores, J.A., Sierro, F.J., Sanchez-Vidal, A. and Calafat, A., 2011. Microplankton response to environmental conditions in the Alboran Sea (Western Mediterranean): One year sediment trap record. Marine Micropaleontology, 78: 14-24.

Juggins, S., 2003. C2 User guide. Software for ecological and palaeoecological data analysis and visualisation. University of Newcastle, Newcastle upon Tyne, UK, 69.

Kageyama, M., Nebout, N.C., Sepulchre, P., Peyron, O., Krinner, G., Ramstein, G. and Cazet, J.-P., 2005. The Last Glacial Maximum and Heinrich Event 1 in terms of climate and vegetation around the Alboran Sea: a preliminary model-data comparison. Comptes Rendus Geoscience, 337: 983-992.

Kucera, M., Rosell-Melé, A., Schneider, R., Waelbroeck, C. and Weinelt, M., 2005b. Multiproxy approach for the reconstruction of the glacial ocean surface (MARGO). Quaternary Science Reviews, 24: 813–819

Kucera, M., Weinelt, M., Kiefer, T., Pflaumann, U., Hayes, A., Weinelt, M., Chen, M.-T., Mix, A.C., Barrows, T.T., Cortijo, E., Duprat, J., Juggins, S. and Waelbroeck, C., 2005a. Reconstruction of sea-surface temperatures from assemblages of planktonic foraminifera: multi-technique approach based on geographically constrained calibration data sets and its application to glacial Atlantic and Pacific Oceans. Quaternary Science Reviews, 24: 951-998.

Kuhlemann, J., Rohling, E., Krumrei, I., Kubik, P., Ivy-Ochs, S. and Kucera, M., 2008. Regional synthesis of Mediterranean atmospheric circulation during the Last Glacial Maximum. Science, 321: 1338–1340.

Locarnini, R., Mishonov, A., Antonov, J., Boyer, T., Garcia, H., Baranova, O., Zweng, M. and Johnson, D., 2010. World Ocean Atlas 2009, vol. 1, Temperature, edited by S. Levitus, 184 pp. US Gov. Print. Off., Washington, DC.

Macías, D., Bruno, M., Echevarría, F., Vázquez, A. and García, C.M., 2008. Meteorologically-induced mesoscale variability of the North-western Alboran Sea (southern Spain) and related biological patterns. Estuarine, Coastal and Shelf Science, 78: 250-266.

Maiorano, P., Marino, M. and Flores, J.A., 2009. The warm interglacial Marine Isotope Stage 31: Evidences from the calcareous nannofossil assemblages at Site 1090 (Southern Ocean). Marine Micropaleontology, 71 166-175.

Martrat, B., Grimalt, J.O., Shackleton, N.J., Abreu, L., Hutterli, M.A. and Stocker, T.F., 2007. Four climate cycles of recurring deep and surface water destabilizations on the Iberian margin. Science, 317: 502 - 507.

Masqué, P., Fabres, J., Canals, M., Sanchez-Cabeza, J.A., Sanchez-Vidal, A., Cacho, I., Calafat, A.M. and Bruach, J.M., 2003. Accumulation rates of major constituents of hemipelagic sediments in the deep Alboran Sea: a centennial perspective of sedimentary dynamics. Marine Geology, 193: 207-233.

McIntyre, A. and Bé, A.W.H., 1967. Modern coccolithophoridae of the Atlantic Ocean. Placoliths and cyrtoliths. Deep Sea Research and Oceanographic Abstracts, 14: 561-597.

McIntyre, A., Bé, A.W.H. and Roche, M.B., 1970. Modern Pacific coccolithophorida: a paleoontological thermometer Transactions of the New York Academy of Sciences, 32: 720-731.

McIntyre, A. and Molfino, B., 1996. Forcing of Atlantic Equatorial and Subpolar Millennial Cycles by Precession. Science, 274: 1867-1870.

Melki, T., 2011. Variation of deepwater convection in the western Mediterranean Sea (Gulf of Lion) during the last 28 ka. Quaternary International, 241: 160-168.

Molfino, B. and McIntyre, A., 1990. Precessional forcing of nutricline dynamics in the equatorial Atlantic. Science, 249: 766-769.

Müller, P.J., Kirst, G., Ruhland, G., von Storch, I. and Rosell-Melé, A., 1998. Calibration of the alkenone paleotemperature index $U_{37}^{K'}$ based on core-tops from the eastern South Atlantic and the global ocean (60°N-60°S). Geochimica et Cosmochimica Acta, 62: 1757-1772.

Navarro, G., Vázquez, Á., Macías, D., Bruno, M. and Ruiz, J., 2011. Understanding the patterns of biological response to physical forcing in the Alborán Sea (western Mediterranean). Geophysical Research Letters, 38.

Okada, H. and Honjo, S., 1973. The distribution of oceanic coccolithophorids in the Pacific. Deep Sea Research and Oceanographic Abstracts, 20: 355-374.

Okada, H. and Wells, P., 1997. Late Quaternary nannofossil indicators of climate change in two deep-sea cores associated with the Leeuwin Current off Western Australia. Palaeogeography, Palaeoclimatology, Palaeoecology, 131: 413-432.

Overpeck, J., Webb III, T. and Prentice, I., 1985. Quantitative interpretation of fossil pollen spectra: dissimilarity coefficients and the method of modern analogs. Quaternary Research, 23: 87-108.

Paillard, D., Labeyrie, L. and Yiou, P., 1996. Macintosh program performs time-series analysis. Eos Transactions American Geophysical Union, 77: 379.

Pérez-Folgado, M., Sierro, F.J., Flores, J.A., Cacho, I., Grimalt, J.O., Zahn, R. and Shackleton, N., 2003. Western Mediterranean planktonic foraminifera events and millennial climatic variability during the last 70 kyr. Marine Micropaleontology, 48: 49-70.

Prell, W.L., 1985. Stability of low-latitude sea-surface temperatures: an evaluation of the CLIMAP reconstruction with emphasis on the positive SST anomalies. Technical Report 25. DOE/ER/60167-1; Other: ON: DE85016190 United StatesOther: ON: DE85016190Wed Feb 06 21:52:10 EST 2008NTIS, PC A04/MF A01; 1.ERA-10-042946; EDB-85-134447English, Washington D.C.

R Development Core Team, 2011. R: A language and environment for statistical computing. R Foundation for Statistical Computing.

Reimer, P.J., Bard, E., Bayliss, A., Beck, J.W., Blackwell, P.G., Bronk Ramsey, C., Grootes, P.M., Guilderson, T.P., Haflidason, H., Hajdas, I., Hatté, C., Heaton, T.J., Hoffmann, D.L., Hogg, A.G., Hughen, K.A., Kaiser, K.F., Kromer, B., Manning, S.W., Niu, M., Reimer, R.W., Richards, D.A., Scott, E.M., Southon, J.R., Staff, R.A., Turney, C.S.M. and van der Plicht, J., 2013. IntCal13 and Marine13 Radiocarbon Age Calibration Curves 0-50,000 Years cal BP. Radiocarbon, 55: 1869-1887.

Rodrigo-Gámiz, M., Martínez-Ruiz, F., Jiménez-Espejo, F.J., Gallego-Torres, D., Nieto-Moreno, V., Romero, O. and Ariztegui, D., 2011. Impact of climate variability in the western Mediterranean during the last 20,000 years: oceanic and atmospheric responses. Quaternary Science Reviews, 30: 2018-2034.

Rodrigo-Gámiz, M., Martínez-Ruiz, F., Rodríguez-Tovar, F.J., Jiménez-Espejo, F.J. and Pardo-Igúzquiza, E., 2014. Millennial- to centennial-scale climate periodicities and forcing mechanisms in the westernmost Mediterranean for the past 20,000 yr. Quaternary Research, 81: 78-93.

Rogerson, M., Cacho, I., Jimenez-Espejo, F., Reguera, M.I., Sierro, F.J., Martinez-Ruiz, F., Frigola, J. and Canals, M., 2008. A dynamic explanation for the origin of the western Mediterranean organic-rich layers. Geochemistry, Geophysics, Geosystems, 9: Q07U01.

Rohling, E.J., Den Dulk, M., Pujol, C. and Vergnaud-Grazzini, C., 1995. Abrupt hydrographic change in the Alboran Sea (western Mediterranean) around 8000

yrs BP. Deep Sea Research Part I: Oceanographic Research Papers, 42: 1609-1619.

Ruiz, J., Echevarría, F., Font, J., Ruiz, S., García, E., Blanco, J.M., Jiménez-Gómez, F., Prieto, L., González-Alaminos, A., García, C.M., Cipollini, P., Snaith, H., Bartual, A., Reul, A. and Rodríguez, V., 2001. Surface distribution of chlorophyll, particles and gelbstoff in the Atlantic jet of the Alborán Sea: from submesoscale to subinertial scales of variability. Journal of Marine Systems, 29: 277-292.

Sarhan, T., García Lafuente, J., Vargas, M., Vargas, J.M. and Plaza, F., 2000. Upwelling mechanisms in the northwestern Alboran Sea. Journal of Marine Systems, 23: 317-331.

Sbaffi, L., Wezel, F.C., Curzi, G. and Zoppi, U., 2004. Millennial- to centennial-scale palaeoclimatic variations during Termination I and the Holocene in the central Mediterranean Sea. Global and Planetary Change, 40: 201-217.

Scherer, R.P., Bohaty, S.M., Dunbar, R.B., Esper, O., Flores, J.A., Gersonde, R., Harwood, D.M., Roberts, A.P. and Taviani, M., 2008. Antarctic records of precession-paced insolation driven warming during early Pleistocene Marine Isotope Stage 31. Geophysical Research Letters, 35: L03505.

Schlitzer, R., 2008. Ocean Data View, http://odv.awi.de.

Schulz, M. and Mudelsee, M., 2002. REDFIT: estimating red-noise spectra directly from 768 unevenly spaced paleoclimatic time series. Computers & Geosciences, 28: 421-426.

Siani, G., Paterne, M., Arnold, M., Bard E, Métivier, B., Tisnerat, N. and Bassinot, F., 2000. Radiocarbon reservoir ages in the Mediterranean Sea and Black Sea. Radiocarbon, 42: 271-280.

Sierro, F.J., Bárcena, M.Á., Flores J. A, Cacho, I., Pelejero, C., Grimalt, J. and Shackleton, N., 1998. Origin of the youngest western Mediterranean organic-rich layer: productivity or stagnation. In: F. Abrantes (Editor), Reconstructing Ocean History, A Window Into the Future. 6th International Conference on Paleoceanography, Lisbon, pp. 211.

Sierro, F.J., Hodell, D.A., Curtis, J.H., Flores, J.A., Reguera, I., Colmenero-Hidalgo, E., Bárcena, M.A., Grimalt, J.O., Cacho, I., Frigola, J. and Canals, M., 2005. Impact of iceberg melting on Mediterranean thermohaline circulation during Heinrich events. Paleoceanography, 20: PA2019.

Stanford, J.D., Rohling, E.J., Bacon, S., Roberts, A.P., Grousset, F.E. and Bolshaw, M., 2011. A new concept for the paleoceanographic evolution of Heinrich event 1 in the North Atlantic. Quaternary Science Reviews, 30: 1047-1066.

Stuiver, M. and Reimer, P.J., 1993. Extended 14C data base and revised CALIB 3.0 14C Age calibration program. Radiocarbon, 35: 215–230.

Telford, R., 2012. palaeoSig: significance tests of quantitative palaeoenvironmental reconstructions. R package version, 1.1-1.

Telford, R.J. and Birks, H.J.B., 2011. A novel method for assessing the statistical significance of quantitative reconstructions inferred from biotic assemblages. Quaternary Science Reviews, 30: 1272-1278.

Telford, R.J., Li, C. and Kucera, M., 2013. Mismatch between the depth habitat of planktonic foraminifera and the calibration depth of SST transfer functions may bias reconstructions. Clim. Past, 9: 859-870.

Thierstein, H.R. and Young, J.R. (Editors), 2004. Coccolithophores: from molecular processes to global impact. Springer, Berlin, 565 pp.

Villanueva, J., Pelejero, C. and Grimalt, J.O., 1997. Clean-up procedures for the unbiased estimation of C37 alkenone sea surface temperatures and terrigenous n-alkane inputs in paleoceanography. Journal of Chromatography A, 757: 145-151.

Weaver, P.P.E. and Pujol, C., 1988. History of the last deglaciation in the Alboran Sea (western Mediterranean) and adjacent north Atlantic as revealed by coccolith floras. Palaeogeography, Palaeoclimatology, Palaeoecology, 64: 35-42.

Wiersma, A.P. and Renssen, H., 2006. Model-data comparison for the 8.2 ka BP event: confirmation of a forcing mechanism by catastrophic drainage of Laurentide Lakes. Quaternary Science Reviews, 25: 63-88.

Winter, A. and Siesser, W.G. (Editors), 1994. Coccolithophores. Cambridge Univ. Press, Cambridge, U. K., 242 pp.

Zanchetta, G., Drysdale, R.N., Hellstrom, J.C., Fallick, A.E., Isola, I., Gagan, M.K. and Pareschi, M.T., 2007. Enhanced rainfall in the Western Mediterranean during deposition of sapropel S1: stalagmite evidence from Corchia cave (Central Italy). Quaternary Science Reviews, 26: 279-286.

APPENDIX. Taxonomic appendix

The list below includes the taxa of calcareous nannoplankton in alphabetical order identified and counted in this study. Some taxa were lumped together as described in the text.

Braarudosphaera bigelowii (Gran & Braarud 1935)

Calcidiscus leptoporus (Murray & Blackman 1898)

Calciosolenia murrayi Gran 1912

Coccolithus pelagicus ssp. *braarudii* (Gaarder 1962)

Coccolithus pelagicus (Wallich 1877) Schiller 1930 ssp. *pelagicus*

Discosphaera tubifera (Murray & Blackman, 1898)

Emiliania huxleyi (Lohmann 1902)

Emiliania huxleyi Type B (*pujosiae*) (> 4 µm)

Florisphaera profunda (Okada & Honjo 1973)

Gephyrocapsa aperta Kamptner 1963

Gephyrocapsa caribbeanica Boudreaux & Hay, in Hay et al. 1967

Gephyrocapsa ericsonii McIntyre & Bé 1967

Gephyrocapsa muellerae Bréhéret 1978

Gephyrocapsa oceanica Kamptner 1943

Helicosphaera spp., (mainly *H. carteri* (Wallich 1877))

Oolithotus fragilis (Lohmann 1912)

Pontosphaera spp. Schiller 1925

Rhabdospahera clavigera Murray & Blackman 1898

Syracosphaera spp. (mainly *S. pulchra*, Lohmann 1902)

Umbellosphaera spp., (mainly *U. tenuis* (Kamptner 1937))

Umbilicosphaera sibogae (Weber-van Bosse 1901)